Control of Inorganic Layer Thickness in Self-Assembled Iron Oxide/Surfactant Composites

Sarah H. Tolbert,[†,‡] Peter Sieger,[†] Galen D. Stucky,*[,†] Sheila M. J. Aubin,[§] Chi-Cheng Wu,[§] and David N. Hendrickson*[,§]

Contribution from the Departments of Chemistry, University of California, Santa Barbara, California 93106-9510, and University of California, San Diego, La Jolla, California 92093

Abstract: The synthesis and characterization of ordered, lamellar, iron oxide/surfactant composites in which the iron oxide layer thickness is selectively varied are presented. These new materials are prepared by the controlled precipitation and hydrolysis of aqueous iron cations into self-assembled iron/surfactant arrays. The use of redox chemistry to alter the solubility of iron oxide and thus control hydrolysis, solubility, and inorganic layer thickness is a key feature of the synthesis procedure. The composites show a layered structure as determined by X-ray diffraction and can be produced with approximately 3 to nearly 20 Å of iron oxide in alternation with surfactant bilayers. For samples with 10 Å or thicker iron oxide layers, magnetic susceptibility measurements and Mössbauer spectroscopy indicate the presence of superantiferromagnetic domain structures with smaller domains observed in samples with thinner layers. The results are a first step toward the simple design of hierarchical nanostructured magnetic materials using cooperative, three-dimensional inorganic/organic self-organization.

I. Introduction

Recent developments in the synthesis of self-assembled inorganic/surfactant composites have opened up a new field in the study of composite materials. These compounds, exemplified by Mobil Corp.'s M41S silica-based composites,[1] tend to show periodicity on the 2−10 nm scale.[1,2] This size range is unique in that many compounds exhibit properties that are intermediate between those observed in isolated molecules and those seen in bulk solids. In addition, the formation of supramolecular assemblies with meso-scale periodicity is an important step in the quest to control periodicity on length scales between atomic and macroscopic dimensions.[3] Recently, the original surfactant/aluminosilicate composites[1,4] have been extended to a variety of transition metal oxides,[5−7] with potential catalytic applications, as well as to multiple combinations of metal oxides and silica.[8−11] The production of surfactant/inorganic composite materials with size-controlled optical

properties has also been achieved.[12] Here we present a new area: inorganic/surfactant composites with size-dependent magnetic properties.

In this paper, the synthesis and characterization of layered iron oxide/surfactant composites are described. Iron oxide was chosen as the inorganic component for a number of reasons. In the first place, iron oxide is the only pure metal oxide to show strong ferrimagnetism at room temperature. While the majority of iron oxide and oxy-hydroxide phases are not ferro- or ferrimagnetic at room temperature, there is some possibility of accessing these potentially important phases.[13] Second, iron shows a range of chemical behavior in aqueous solution.[14,15] This diversity allows us to chose conditions which will favor specific products. Finally, aqueous iron has an easily accessible redox equilibrium: $Fe(II) \leftrightarrow Fe(III)$.[14] This feature is key to the synthesis scheme presented below as it allows the solution phase behavior of iron ions to be altered in a dramatic and well-defined way.

The above ideas were combined to produce lamellar iron oxide/surfactant composites consisting of surfactant layers, alternating with approximately one, two, three, or six layers of iron oxide. The layer thickness is controlled by the differential solubility of Fe(II) and Fe(III) in aqueous solutions coupled with our ability to chemically convert between these species. The composites were characterized structurally by powder X-ray diffraction, compositionally by elemental analysis, and chemically (oxidation state) by Mössbauer spectroscopy. Both

† University of California, Santa Barbara.
‡ Permanent address: Department of Chemistry and Biochemistry, University of California, Los Angeles, CA 90095-1569.
§ University of California, San Diego.
⊗ Abstract published in *Advance ACS Abstracts,* August 1, 1997.
(1) Kresge, C. T.; Leonowitz, M. E.; Roth, W. J.; Vartuli, J. C.; Beck, J. S. *Nature* **1992,** *359,* 710. Beck, J. S.; Vartuli, J. C.; Roth, W. J.; Leonowicz, M. E.; Kresge, C. T.; Schmitt, K. T.; Chu, C. T.-W.; Olson, D. H.; Sheppard, E. W.; McCullen, S. B.; Higggins, J. B.; Schlenker, J. L. *J. Am. Chem. Soc.* **1992,** *114,* 10834.
(2) Huo, Q.; Margolese, D. I.; Stucky, G. D. *Chem. Mater.* **1996,** *8,* 1147.
(3) Huo, Q.; Feng, J. L.; Schuth, F.; Stucky, G. D. *Chem. Mater.* **1997,** *9,* 14. Schacht, S.; Huo, Q.; Voigtmartin, I. G.; Stucky G. D.; Schuth, F. *Science* **1996,** *273,* 768.
(4) Firouzi, A.; Kumar, D.; Bull, L. M.; Besier, T.; Sieger, P.; Huo, Q.; Walker, S. A.; Zasadzinski, J. A.; Glinka, C.; Nicol, J.; Margolese, D.; Stucky, G. D.; Chmelka, B. F. *Science* **1995,** *267,* 1138. Huo, Q.; Margolese, D. I.; Ciesla, U.; Feng, P.; Geir, T. E.; Sieger, P.; Leon, R.; Petroff, P. M.; Schüth, F.; Stucky, G. D. *Nature* **1994,** *368,* 317.
(5) Antonelli D. M.; Nakahira, A.; Ying, J. Y. *Inorg. Chem.* **1996,** *35,* 3126. Antonelli D. M.; Ying, J. Y. *Chem. Mater.* **1996,** *8,* 874. Antonelli D. M.; Ying, J. Y. *Angew. Chem., Int. Ed. Engl.* **1996,** *35,* 426. Antonelli, D. M.; Ying, J. Y. *Angew. Chem., Int. Ed. Engl.* **1995,** *34,* 2014.
(6) Ciesla, U.; Schacht, S.; Stucky, G. D.; Unger, K. K.; Schuth, F. *Angew. Chem., Int. Ed. Engl.* **1996,** *35,* 541.
(7) Abe, T.; Taguchi, A.; Iwamoto, M. *Chem. Mater.* **1995,** *7,* 1429.
(8) Morey, M.; Davidson, A.; Ekert, H.; Stucky, G. D. *Chem. Mater.* **1996,** *8,* 486. Morey, M.; Davidson, A.; Stucky, G. D. *Micropor. Mater.* **1996,** *6,* 99.
(9) Corma, A.; Mavarro, M. T.; Perez-Pariente, J. *J. Chem. Soc., Chem. Commun.* **1994,** 147.
(10) Tanev, P. T.; Chibwe, M.; Pinnavaia, T. J. *Nature* **1994,** *368,* 321.
(11) Reddy, K. M.; Moudrakovski, I.; Sayari, A. *J. Chem. Soc., Chem. Commun.* **1994,** 1059.
(12) Braun, P. V.; Osenar, P.; Stupp, S. I. *Nature* **1996,** *380,* 325.
(13) Misawa, T.; Kyuno, T.; Suëtaka, W.; Shimodaira, S. *Corrosion Sci.* **1971,** *11,* 35.
(14) Misawa, T.; Hashimoto, K.; Shimodaira, S. *Corrosion Sci.* **1974,** *14,* 131.
(15) Misawa, T. *Corrosion Sci.* **1973,** *13,* 659.

magnetic susceptibility and Mössbauer spectroscopy are used to analyze the magnetic structure in these materials. The result is a consistent picture of these new materials in terms of both the physical and magnetic structures.

The composites described in this report are divided into three groups (I, II, and III). The detailed structure of each group will be discussed in turn. Group I compounds contain one layer of Fe(II) ions, alternating with a double layer of anionic surfactant molecules (alkyl sulfates in most cases). These materials are similar to Fe(II)/surfactant salts, as exemplified by the fact that the layer spacing and thus the surfactant chain structure is altered upon dehydration. Group II compounds consist of two layers of Fe(III) oxide, alternating with a double layer of anionic surfactant molecules. These compounds have characteristics of Fe(III)/surfactant salts, most notably a change in layer spacing upon dehydration. The final group III compounds consist of approximately three or six layers of iron-(III) oxide in alternation with a double layer of surfactant molecules. These compounds are made by precipitating Fe-(III) from solution into the group I salts described above. Unlike the group I and II compounds, the group III materials are not salt-like, and appear to consist of cross-linked iron oxide layers. The layer thickness is controlled by varying the strain and diffusion length which is in turn accomplished by changing the surfactant hydrophobic tail length. Because a variety of surfactant tail lengths can be employed (in groups I, II, and III), the net result is a system where both the iron oxide layer thickness and the surfactant layer thickness can be varied over a fairly wide range.

II. Experimental Section

Synthesis. Group I Fe(II) salts were made by mixing 20 mL of diluted aqueous solutions of sodium n-alkyl sulfates, $C_nH_{2n+1}OSO_3Na$ ($n = 10, 12, 14, 16, 18$; $c = 0.01-0.05$ mol·L^{-1}), with 20 mL of 0.25 mol·L^{-1} Fe(II) (either from FeCl$_2$ or FeSO$_4$). All solutions were deoxygenated before mixing, and all syntheses were carried out under inert atmosphere to prevent oxidation of Fe(II) to Fe(III). C_nH_{2n+1}-OSO$_3$Na ($n = 16, 18$) solutions were not soluble at this concentration at room temperature; thus, these iron and surfactant solutions were mixed at slightly elevated temperatures (≈ 50 °C). Shortly after mixing, a white precipitate began to form. Formally, these composites are obtained by a simple cation exchange of the surfactant molecules. The precipitate was filtered under argon, washed with deoxygenated water, and dried either under flowing Ar or under vacuum. Dry composites could be exposed to air without oxidation. Meaningful yields were not determined for these materials because of sample losses due to filtering under inert atmosphere. Group II compounds were synthesized by similar means, although in this case, FeCl$_3$ or Fe$_2$(SO$_4$)$_3$ was used as the iron source. The syntheses were not carried out under inert atmosphere, and the final polycrystalline product exhibited a yellow color. Yields ranged from 93 to 96%, indicating that complexation of the anionic surfactant molecules with the highly charged Fe cations is energetically quite favorable.

Dehydration of both group I and group II compounds was accomplished by heating the compounds between 80 and 120 °C or by exposing them to vacuum on the order of 10 mTorr. The dehydration process was fully reversible; samples left at room temperature and normal atmosphere overnight recovered their original hydrated structure.

The group III compounds were synthesized by adding H$_2$O$_2$ to the group I compounds described above in the presence of excess aqueous Fe^{2+}. Two to four milliliters of a 0.88 mol·L^{-1} H$_2$O$_2$ solution was added to the precipitated mixture of C$_n$H$_{2n+1}$OSO$_3$Na and Fe(II) ions. Upon oxidation, a change in the precipitate color from white to brown was observed. Addition of insufficient H$_2$O$_2$ produced a mixture of group I and group III compounds; additions of excess H$_2$O$_2$ produced group III composites in combination with bulk Geothite[16] and Akaganeite[17] (α- and β-FeO(OH)). H$_2$O$_2$ was added under inert atmosphere,

and the solutions were allowed to sit in contact with the mother solution for approximately 12 h before being filtered and washed with water. Samples were filtered and dried in air at room temperature. Yields of these materials ranged from 90 to nearly 100% (calculated on the basis of the initial surfactant concentration and the results of elemental analysis), indicating that surfactant was not lost to solution as the inorganic layer thickness increased. Group III samples were hydrogen treated by heating under flowing H$_2$/Ar (5/95) in a tube furnace. Samples were heated for 10 h at a temperature of 80 °C. Higher temperatures significantly degraded the periodicity of the samples.

Compounds similar to those described above could also be made using a variety of other metal ions and anionic surfactants. Salt-like, iron-based materials could be produced using n-alkyl sulfonates, phosphates, phosphonates, or carboxylates. Non-iron-based salts were also produced. In particular, either the Fe(II) or the Fe(III) solutions employed in group I and group II compounds could be replaced by a variety of other transition metal cations, such as Ni^{2+}, Co^{2+}, Mn^{2+}, Cr^{3+}, and Ti^{4+}. All of these materials form hydrates, changing their structure upon dehydration in the way described above. n-Alkyl phosphate/Fe(II) complexes could be oxidized with H$_2$O$_2$. No changes, except a loss in crystallinity, were observed for all other Fe(II)/surfactant composites after H$_2$O$_2$ treatment. In addition, other metal ions, such as Co(II), Ni(II), Mn(II), and Cr(III), were resistant to oxidation by H$_2$O$_2$, consistent with the large oxidation potentials of these metals and the moderate reduction potential of H$_2$O$_2$ at neutral or slightly acidic pH.

Structural Characterization. Structures were determined using power X-ray diffraction (XRD). A Scintag PAD-X automated diffractometer equipped with a Ge solid-state detector was employed in a $\theta-\theta$ geometry. Data were usually collected from 1.5° to 30° 2θ. For all experiments, we used a flat-plate sample and copper Kα radiation. The overall composition was determined by elemental analysis. Samples were analyzed for carbon, hydrogen, iron, and sulfur content by the UC Berkeley Micro Analytical Laboratory.

Magnetochemistry. The chemical oxidation state and the nature of magnetic exchange interactions were analyzed using magnetic susceptibility and ^{57}Fe Mössbauer spectroscopy. Direct current magnetic susceptibility data on group I and II compounds were collected on a Quantum Design MPMS SQUID susceptometer equipped with a 55 kG magnet and operating in the temperature range 1.8−400 K.[18] Pascal's constants[19] were used to estimate the diamagnetic corrections for each complex which were subtracted from experimental susceptibilities to give the molar paramagnetic susceptibilities. Susceptibility measurements on group III compounds were carried out using a Quantum Design MPMS-5S SQUID susceptometer.[20] Samples consisted of 6−14 mg of composite held between two cotton plugs in a gel capsule. Data were collected from −50 to 50 kG and from room temperature down to 1.7 K. Data included magnetization as a function of field at various temperatures and both field-cooled and zero-field-cooled magnetization at multiple fields. Variable-temperature Mössbauer spectra were obtained in vertical transmission geometry using a constant-acceleration spectrometer that has been described before.[21] The sample temperature was controlled by a Lake Shore Cryotronics Model DRC80C temperature controller in conjunction with a silicon diode mounted on the copper sample cell holder; the system is estimated to have an absolute accuracy of ±3K. Isomer shift values are reported relative to iron foil at 298 K and are not corrected for the temperature-dependent second-order Doppler shift.

III. Results

In this section, the experimental evidence used to assign the structures of groups I, II, and III compounds is presented. In particular, data from direct structural techniques, such as X-ray

(16) JCPDS-ICDD powder pattern card #29-713, 1992.

(17) JCPDS-ICDD powder pattern card #34-1266, 1992.

(18) Measurements carried out at the University of California, San Diego.

(19) *Theory and Applications of Molecular Paramagnetism*; Bordreaux, E. A., Mulay, L. N., Eds.; J. Wiley & Sons: New York, 1976.

(20) Measurements carried out at the University of California, Santa Barbara.

(21) Cohn, M. J.; Timken, M. D.; Hendrickson, D. N. *J. Am. Chem. Soc.* **1984**, *106*, 6.

Table 1.   Layer Spacings from X-ray Powder Diffraction for Iron Oxide/Surfactant Composites

surfactant ($NaC_nH_{2n+1}OSO_3$)	composite formula	layer spacing (Å)^a $d_{(001)}$
	Group I: Fe(II) Salts	
$n = 10, 12, 14, 16, 18$	$Fe(C_nH_{2n+1}OSO_3)_2 \cdot 6H_2O$	18.5 (10),^{b} 20.6 (12),^{b} 23.0 (14),^{b} 26.5 (16), 27.5 (18)
	$Fe(C_nH_{2n+1}OSO_3)_2$ (dehydrated)	28.1 (10), 32.7 (12), 36.0 (14), 41.6 (16), 45.6 (18)
	Group II: Fe(III) Salts	
$n = 10, 12, 14, 16, 18$	$Fe_2O(C_nH_{2n+1}OSO_3)_4 \cdot (8-10)H_2O$	23.1 (12), 26.0 (14), 28.1 (16), 31.0 (18)
	$Fe_2O(C_nH_{2n+1}OSO_3)_4$ (dehydrated)	37.1 (12), 42.5 (14), 46.8 (16), 52.0 (18)
	Group III: Layered Composites	
$n = 10, 12, 14$	$Fe_{6\pm\delta}O_x(OH)_y(C_nH_{2n+1}OSO_3)_2 \cdot zH_2O$	32.8 (10), 36.6 (12), 39.2 (14)
$n = 16, 18$	$Fe_{3\pm\delta}O_x(OH)_y(C_nH_{2n+1}OSO_3)_2 \cdot zH_2O$	31.8 (16), 34.4 (18)

^{a} Esd of d_{100} spacing is ±0.5 Å. ^{b} See ref 22.
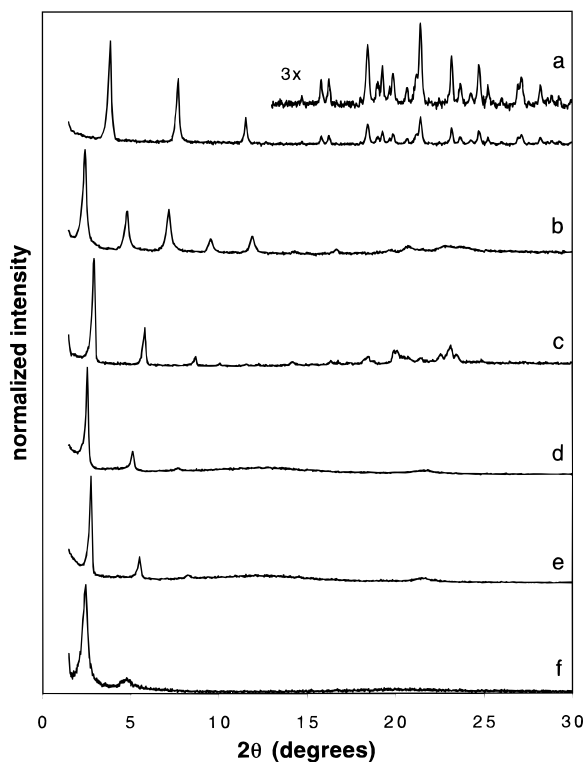
Figure 1. X-ray diffraction from various iron oxide/surfactant composites: (a) Group I, hydrated, $Fe(II)(C_{14}H_{29}OSO_3)_2 \cdot 6H_2O$. (b) Group I, dehydrated, $Fe(II)(C_{14}H_{29}OSO_3)_2$. (c) Group II, hydrated, $Fe(III)_2O(C_{16}H_{33}OSO_3)_4 \cdot (8-10)H_2O$. (d) Group III, $Fe(III)_{3\pm\delta}O_x(OH)_y(C_{18}H_{37}OSO_3)_2 \cdot zH_2O$. (e) Group III, $Fe(III)_{3\pm\delta}O_x(OH)_y(C_{16}H_{33}OSO_3)_2 \cdot zH_2O$. (e) Group III, $Fe(III)_{6\pm\delta}O_x(OH)_y(C_{12}H_{25}OSO_3)_2 \cdot zH_2O$.
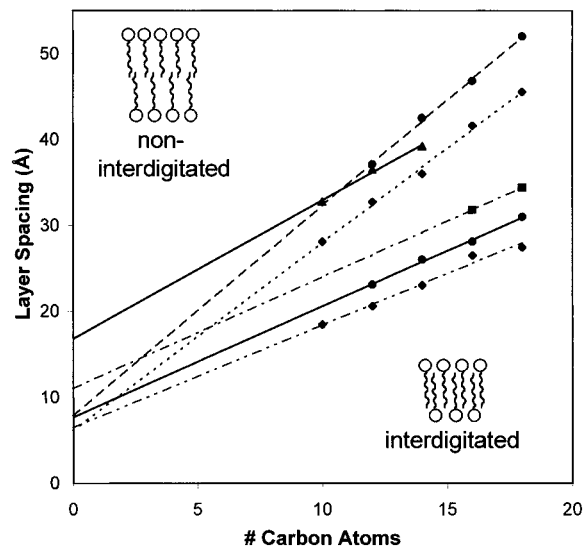

Figure 2. Change in lamellar d spacing with surfactant carbon chain length. Data are presented for hydrated and dehydrated group I and II compounds and for three- and six-layered group III compounds. The slopes of these lines indicate whether the surfactant chains are interdigitated; the y intercept is a measure of the thickness of the iron oxide layer plus the surfactant headgroup. Legend: ($\blacklozenge$) group I, hydrated; ($- - -$) group I, hydrated, fit; ($\blacklozenge$) group I, dehydrated; (- - -) group I, dehydrated, fit; ($\bullet$) group II, hydrated; ($-$) group II, hydrated, fit; ($\bullet$) group II, dehydrated; ($- - -$) group II, dehydrated, fit; ($\blacktriangle$) group III, six layer; ($-$) group III, six layer, fit; ($\blacksquare$) group III, three layer; ($- \cdot -$) group III, three layer, fit.

diffraction, are combined with probes of magnetic structure, such as magnetic susceptibility, to produce a self-consistent picture of both the local bonding and magnetic exchange coupling, and the superstructure and magnetic domain structure in these inorganic/organic composites. Group I, II, and III compounds will be discussed in order, and we will emphasize the defining characteristics of each class of materials.

Group I Compounds. Powder XRD data (Figure 1, a and b) clearly demonstrate the layered structure of these compounds: a series of equally spaced peaks are observed in the low-angle regime. This progression is observed in both the hydrated (Figure 1a) and dehydrated (Figure 1b) forms of group I salts, showing that the layered structure is a general feature of these composites. In the hydrated salts, narrow well-resolved peaks are also seen in the high-angle regime, indicating that in these compounds the overall layered structure is accompanied by atomic scale ordering and registry of the layers.[22] The dramatic change in structure upon dehydration is a key feature that allows us to describe these Fe(II) compounds as salts. The dehydrated structures show primary layer spacings (d_{001}) that

are significantly larger than those observed in the hydrated compounds: the ratio of the d_{001} spacing of the dehydrated and hydrated phases is $r = d_{001}(dehyd)/d_{001}(hyd) = 1.6 \pm 0.1$. Layer spacings for a range of hydrated and dehydrated group I compounds made with surfactants containing 10−18 carbons are presented in Table 1.

The change in surfactant chain packing upon dehydration can be understood through analysis of the variation in fundamental layer spacing (d_{001}) with surfactant chain length. For a typical aliphatic chain, an increase of 1.26−1.27 Å in length is observed upon the addition of one carbon atom.[23] The change in d spacing with each added carbon atom is thus a measure of the chain packing.[23] Samples that show a slope of 1.27 Å/carbon atom in a plot of lamellar layer spacing versus surfactant chain length can be considered interdigitated layers (Figure 2) with the carbon atom chains all arranges normal to the plane of the layer (frequently referred to as a paraffin-type monolayer.[24]).

(22) X-ray diffraction patterns fully indexed−monoclinic symmetry: $n = 10$, $a = 5.42(1)$ Å, $b = 18.06(2)$ Å, $c = 18.67(2)$ Å, $\beta = 93.8(2)°$; $n = 12$, $a = 5.429(6)$ Å, $b = 18.07(2)$ Å, $c = 20.98(2)$ Å, $\beta = 93.55(8)°$; $n = 14$, $a = 5.45(1)$ Å, $b = 18.00(5)$ Å, $c = 22.45(5)$ Å, $\beta = 92.8(4)°$.

(23) Weiss, A. In *Organic Geochemistry*; Eglinton, G., Ed.; Springer: Berlin, 1969; pp 737−781.

Table 2. Slope and Intercept Values Obtained from Fits to the Variation in Lamellar Layer Spacings with Surfactant Carbon Chain Length

	group I: hyd[a]	group I: dehyd[a]	group II: hyd	group II: dehyd	group III: $\approx$6 layers[b]	group III: $\approx$3 layers[b]
intercept (Å)	6.5	6.1	7.7	7.9	16.8	11
slope (Å/C atom)	1.20	2.19	1.29	2.45	1.61	1.30

[a] hyd = hydrated; dehyd = dehydrated. [b] Note that these values are determined from only 2 (3-layer) and 3 (6-layer) data points, and thus are susceptible to error.

Tilting the aliphatic chains results in a reduction of the slope from the value of 1.27 Å/carbon atom. A completely noninterdigitated bilayer (paraffin-type bilayer, Figure 2) with the chains normal to the plane of the layers should produce a value of 2.52 Å/carbon atom (twice 1.26) for the slope.[23] Tilting the aliphatic chains or partial interdigitation of the chains results in a value between 1.27 and 2.52 Å/carbon atom. Using these same arguments, the intercept of the *d* spacing versus carbon chain length plot can be assigned to the thickness of the inorganic layer plus the surfactant headgroup. In these experiments, however, the intercept values have significant errors associated with them (on the order of 20%) because of the long extrapolation to zero carbons.

The *d* spacing (in angstrom) plotted against the number of carbon atoms in the sulfate surfactants for group I, II, and III compounds is presented in Figure 2. Group I compounds are indicated by diamond symbols along with linear fits to the data; Table 2 contains slope and intercept values for these fits. Figure 2 and Table 2 both indicate a significantly greater slope for the dehydrated group I samples (slope = 2.19 Å/carbon atom), compared to the hydrated material (slope = 1.20 Å/carbon atom). The hydrated material is thus shown to be composed of interdigitated surfactant chains with only a slight tilt of the alkyl chain. The dehydrated material, in contrast, is mostly noninterdigitated, although some interdigitation or chain tilt must be invoked to account for the difference between the observed value of 2.19 Å/carbon atom and the ideal value of 2.52 Å/carbon atom. The change in chain packing can upon dehydration can be understood by considering the radius of the hydrated and dehydrated Fe(II) ion. The hydrated species is large, and thus, interdigitation of the surfactant tails allows the surfactant headgroups to be spaced well apart. The dehydrated ion is much smaller and thus a paraffin-type bilayer, in which the surfactant headgroups are much closer to each other and the surfactant tails are not interdigitated, is favored.

Because of the ease with which these compounds are dehydrated, isolated Fe(II) ions are predicted for group I compounds. This assertion is confirmed by both magnetic susceptibility and ^{57}Fe Mössbauer data. Mössbauer spectra (data not shown) indicate the presence of only high-spin Fe(II). The magnetic susceptibility data, (Figure 3a) plotted as $\chi_M T$ versus *T*, exhibit temperature-independent behavior in the range of 320−20.0 K ($\chi_M T = 3$ cm^3 K mol^{-1} or μ_{eff}/unit = 5.0 μ_B). This observation is consistent with the presence of only monomeric, high-spin Fe^{2+} ions. The decrease in $\chi_M T$ at temperatures below about 20 K is most likely attributable to single-ion zero-field splitting expected for high-spin Fe^{2+} ions.

Elemental analysis of the hydrated material synthesized with a 12-carbon surfactant shows a C:H:S:Fe wt % ratio of 41.9: 9.1:9.3:8.3. These results indicate a surfactant:Fe molar ratio of 2.0:1.0. If the weight balance is assumed to be oxygen, the
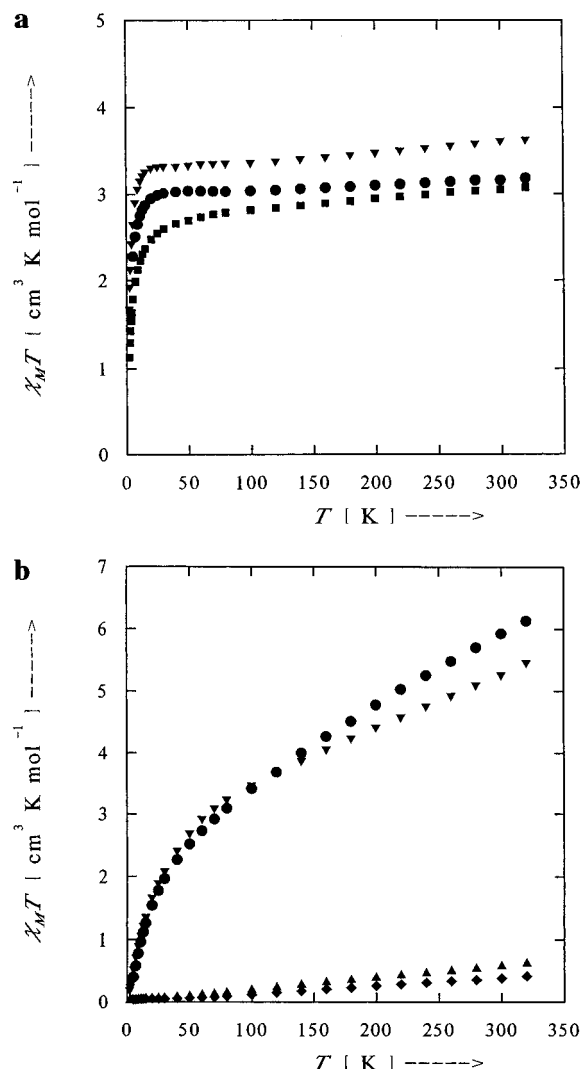
(24) Vaya, R. A.; Teukolsky, R. K.; Gianelis, E. P. *Chem. Mater.* **1994**, *6*, 1017 and references therein.

Figure 3. (a) Magnetic susceptibility plotted as the product of the molar paramagnetic susceptibility with temperature ($\chi_M T$) versus temperature for group I compounds: (●) Fe(II)(C$_{12}$H$_{25}$OSO$_3$)$_2$·6H$_2$O, (■) Fe(II)(C$_{16}$H$_{33}$OSO$_3$)$_2$·6H$_2$O, (▼) Fe(II)(C$_{18}$H$_{37}$OSO$_3$)$_2$·6H$_2$O. (b) Magnetic susceptibility plotted as the product of the molar paramagnetic susceptibility with temperature ($\chi_M T$) versus temperature for group II and III compounds. Group II: (◆) Fe(III)$_2$O(C$_{12}$H$_{25}$OSO$_3$)$_4$·(8−10)-H$_2$O, (▲) Fe(III)$_2$O(C$_{18}$H$_{37}$OSO$_3$)$_4$·(8−10)H$_2$O. Group III: (▼) Fe-(III)$_{3\pm\delta}$O$_x$(OH)$_y$(C$_{18}$H$_{37}$OSO$_3$)$_2$·zH$_2$O, (●) Fe(III)$_{6\pm\delta}$O$_x$(OH)$_y$(C$_{12}$H$_{25}$-OSO$_3$)$_2$·zH$_2$O.

postulate of isolated, monomeric Fe^{2+} from magnetic susceptibility can be used to show that there are approximately 5.5 waters of hydration per iron atom. Corroborating this conclusion, dehydration experiments on carefully hydrated group I compounds made with 12-carbon surfactants show a weight loss of 15.5% which is in excellent agreement with a value of 15.6% corresponding to the loss of six water molecules per iron atom. The general formula for these group I materials is thus Fe(II)-(C$_n$H$_{2n+1}$OSO$_3$)$_2$·6H$_2$O (n = 10−18).

Group II Compounds. Group II compounds also exhibit a lamellar progression in XRD (Figure 1c). As observed for the group I materials, these compounds show a dramatic change in structure upon dehydration [d_{001}(dehyd)/d_{001}(hyd) is again 1.6 ± 0.1], with a layer spacing change of 1.29 Å/carbon atom observed for hydrated samples and 2.45 Å/carbon atom seen in the dehydrated material (Table 2). These results are, as noted earlier, consistent with mostly interdigitated surfactant chains in the hydrated material and non-interdigitated chains in the dehydrated phase. Little chain tilt is indicated in either phase,

and good agreement is seen between the zero-carbon intercepts for hydrated and dehydrated compounds (Table 2). Like the group I materials, no atomic scale ordering is observed in the dehydrated material. Additionally, the hydrated phases here show only poorly defined atomic level ordering compared to group I hydrated salts, as indicated by the broader high-angle diffraction peaks in Figure 1c. Layer spacings for a range of hydrated and dehydrated group II compounds, prepared with sulfate surfactants containing 12−18 carbon atoms, are presented in Table 1.

Magnetic susceptibility data can be used to understand the overall structure of these composites. Mössbauer spectroscopy data show that these samples contain only Fe(III) ions [data not shown], which is consistent with the use of Fe^{3+} as the starting material. In contrast to group I compounds, magnetic susceptibility data for group II materials (Figure 3b) no longer indicate isolated paramagnetic ions. As shown in Figure 3b, the values of $\chi_M T$ are relatively small for these complexes. For example, in the complex synthesized with $C_{12}H_{25}OSO_3^-$ surfactant, $\chi_M T$ decreases with decreasing temperature from 0.424 cm^3 K mol^{-1} (μ_{eff}/unit = 1.84 μ_B) at 320 K to 0.0367 cm^3 K mol^{-1} (0.54 μ_B) at 4.51 K. These plots of $\chi_M T$ vs T are quite similar to those expected for a complex with two high-spin Fe^{3+} ions bridged by an oxide anion,[25,26 27] In such an $[Fe_2(\mu\text{-O})]^{4+}$ unit there is a relatively strong antiferromagnetic exchange interaction that leads to an appreciable decrease in the $\chi_M T$ value compared to that expected for two noninteracting, high-spin Fe^{3+} ions. The dinuclear $[Fe_2(\mu\text{-O})]^{4+}$ unit has a diamagnetic $S = 0$ ground state; only this $S = 0$ state is thermally populated at temperature below ca. 100 K.

Consistent with the formal charge on the postulated $[Fe_2(\mu\text{-O})]^{4+}$ unit, elemental analysis indicates a surfactant:iron molar ratio of 2.0:1.0, indicating that four surfactant molecules are associated with each $[Fe_2(\mu\text{-O})]^{4+}$ unit. The increased d spacing (∼2.7 Å) observed for group II compounds, relative to group I materials, however, indicates that the $[Fe_2(\mu\text{-O})]^{4+}$ unit is oriented with its long axis perpendicular to the lamellar planes. This orientation is also consistent with the facile dehydration of these materials; if the long axis of the $[Fe_2(\mu\text{-O})]^{4+}$ unit was parallel to the lamellar planes, this would lock the spacing between surfactant headgroups and hinder rearrangement of the surfactants upon dehydration. Assuming these compounds contain only C, H, S, Fe, and O, an overall C:H:S:Fe wt % ratio of 41.9:9.0:9.6:8.2 for a hydrated sample synthesized with a 12-carbon surfactant indicates four to five H_2O molecules per Fe atom. This is confirmed by dehydration experiments which show a weight loss of 11% upon dehydration in group II compounds synthesized with 12-carbon surfactants; this again corresponds to the loss of four to five H_2O molecules per Fe atom. The most probable overall structure of these compounds is thus $Fe(III)_2O(C_nH_{2n+1}OSO_3)_4 \cdot (8-10)H_2O$ ($n = 12-18$).

Group III Compounds. Group III compounds are formed from group I salts by oxidation with H_2O_2 in the presence of excess Fe^{2+} (Figure 1d−f). The oxidation is accompanied by a significant increase in layer spacing. These materials retain the long-range lamellar ordering observed in group I and II compounds (low-angle diffraction) but show no signs of atomic scale order (high-angle diffraction). This observation is consistent with a structure composed of cross-linked iron oxide layers comprised of small, randomly oriented domains, in alternation with disordered surfactant bilayers. Corroborating

this idea is the fact that group III compounds show no change in d_{001} spacing upon dehydration; the distance between surfactants seems to be fixed by bonding to a rigid iron oxide layer.

A comparison of group I and group III compounds made with the same surfactant provides insight into the structural changes occurring upon oxidation. In compounds synthesized using 16- or 18-carbon surfactants ($C_nH_{2n+1}OSO_3$, $n = 16, 18$), the d_{001} spacing increases by about 6 Å in the group III materials compared to the group I phases. This is approximately twice the O−Fe−O distance found in many of the bulk iron oxide and iron oxy-hydroxide compounds ($d = 2.7-3.1$ Å).[28] In compounds synthesized with 10-, 12-, or 14-carbon surfactants ($C_nH_{2n+1}OSO_3$, $n = 10, 12, 14$), increases of approximately 15.5 Å, or 5 times the bulk O−Fe−O distance, are observed. Comparison of group II and group III layer spacings shows a similar trend with a one O−Fe−O layer distance increase observed for 16- and 18-carbon surfactants and a four O−Fe−O layer spacing increase observed for 12- and 14-carbon surfactants. This same trend is also observed when comparing the zero-carbon intercepts of group III compounds with group I or II material (Figure 2 and Table 2), although the absolute values of the layer spacings that can be obtained from that data are less accurate than those presented above due to errors associated with the extrapolation to zero chain length. Examination of the slopes from group III compounds (Table 2) additionally indicates that the surfactant tails are mostly, but not completely, interdigitated as both values are slightly greater than 1.26 Å/carbon atom. The large errors associated with linear fits to only two or three data points prevent more detailed interpretation of these data.

We thus conclude that group III compounds made with 10-, 12-, and 14-carbon sulfate surfactants consist of approximately six iron oxide layers in alternation with mostly interdigitated surfactant bilayers. Group III compounds made with 16- and 18-carbon surfactants consist of roughly three iron oxide layers, again in alternation with mostly interdigitated surfactant bilayers. Elemental analyses[29] corroborate this idea, although some deviations from 2:6 and 2:3 surfactant:Fe molar ratios are observed (surfactant:Fe = 2.0:6.6, 2.0:3.8, and 2.0:3.5 for $C_nH_{2n+1}OSO_3$, $n = 12, 16,$ and 18, respectively). The excess Fe in all these materials is possibly in the form of a small amount of bulk FeO(OH). Corroborating this idea, a weak peak at approximately 22° 2θ which can be assigned to the FeO(OH) structure is sometimes observed in these materials.[30]

Mössbauer spectroscopy and magnetic susceptibility measurements are key to understanding the inorganic structures of these group III compounds. High-temperature Mössbauer studies show that all of the iron atoms in these complexes are in the form of high-spin Fe(III) ions [Figure 4, top]; no signal is observed from Fe(II) ions. Magnetic susceptibility data (Figure 3b) provide further information: the value of $\chi_M T$ for the compound consisting of six iron oxide layers in alternation with 12-carbon surfactants decreases gradually from 6.13 cm^3 K mol^{-1}/unit (7.00 μ_B) at 320 K to 2.51 cm^3 K mol^{-1}/unit (4.48

(25) Murray, K. S. *Coord. Chem. Rev.* **1974**, *12*, 1.
(26) Ou, C. C.; Wollman, R. G.; Hendrickson, D. N.; Potenza, J. A. *J. Am. Chem. Soc.* **1978**, *100*, 4717.
(27) Gomez-Romero, P.; Witten, E. H.; Reiff, W. M.; Jameson, G. B. *Inorg. Chem.* **1990**, *29*, 5211.
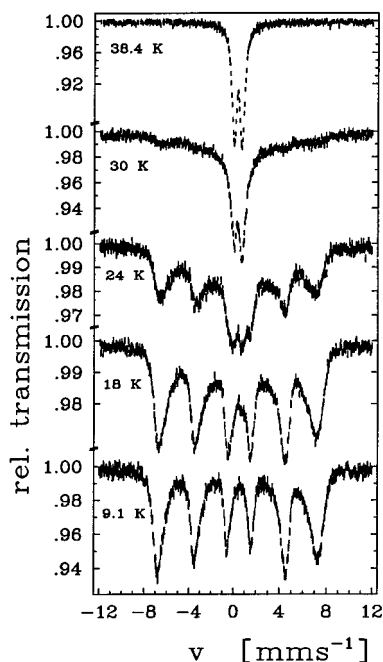
(28) Flynn, C. M. *Chem. Rev. (Washington, D.C.)* **1984**, *84*, 31. Schwertmann, U.; Cornell, R. M. *Iron Oxides in the Laboratory: Preparation and Characterization*; VCH: Weinheim, Germany, 1991 and references therein.
(29) C:H:S:Fe wt % ratios for group III compound synthesized with 12-, 16-, and 18-carbon surfactant molecules are as follows: 12 carbon atoms, 25.0:5.8:5.4:32.0; 16 carbon atoms, 38.8:7.9:5.2*:21.6 (* probably low); 18 carbon atoms, 40.2:8.2:6.1:18.2.
(30) Very small amounts of bulk FeO(OH) do not appear to affect the magnetic measurements presented here. Larger quantities of FeO(OH), however, can be detected in both the magnetic susceptibility and Mössbauer spectroscopy of contaminated three- and six-layered materials. The signs of bulk FeO(OH) include ZFC/FC divergence points and residual six-peak Mössbauer patterns at temperatures above 100 K.

Layer Thickness in Iron Oxide/Surfactant Composites

J. Am. Chem. Soc., Vol. 119, No. 37, 1997 8657

Figure 4. ^{57}Fe Mössbauer spectra of the group III complex Fe-$(III)_{6\pm\delta}O_x(OH)_y(C_{12}H_{25}OSO_3)_2 \cdot zH_2O$ as a function of temperature. At high temperatures, a doublet indicating high-spin Fe(III) is seen. At lower temperatures, a sextet typical of blocked magnetic domains is observed.

μ_B) at 50.0 K and then more rapidly to 0.404 cm^3 K mol^{-1}/unit (1.80 μ_B) at 5.00 K. This behavior is characteristic of antiferromagnetic exchange interactions between iron ions. If there were no interactions between the six high-spin Fe^{3+} ions in the complex, a value of $\mu_{eff} = 14.5$ mB per complex would be expected. Pairwise Fe$^{3+}\cdots$Fe^{3+} antiferromagnetic interactions, however, give rise to many different spin states. As the temperature is decreased, the populations of states with larger total spin values decrease, while states with smaller spin values become increasingly populated. The observed temperature dependence of $\chi_M T$ is thus consistent with significant antiferromagnetic coupling, as is often observed in FeO(OH) materials.[31]

An understanding of the domain structure within the iron oxide layers can be gained using low-temperature magnetic susceptibility and Mössbauer spectroscopy. In particular, a comparison of temperature-dependent magnetization curves obtained on samples cooled in the absence [zero-field-cooled (ZFC)] or presence [field-cooled (FC)] of a magnetic field can give an indication of the magnetic domain structure. At high temperatures, very small magnetic domains tend to reorient freely to follow an applied magnetic field; this phenomena is known as superparamagnetism.[32] As the temperature is decreased, these domains will eventually pin to the lattice so that, below the blocking temperature (T_B), they are locked and cannot reorient.[33] Samples cooled in the presence of a magnetic field will freeze such that magnetic domains are aligned with the applied field and thus will show a smooth decrease in magnetization with increasing temperature. Samples cooled to temperatures below T_B in the absence of an applied field will freeze with the magnetic domains oriented at random directions, producing a low overall magnetization. As the sample is heated to T_B, the spins will rotate freely and will align with the applied
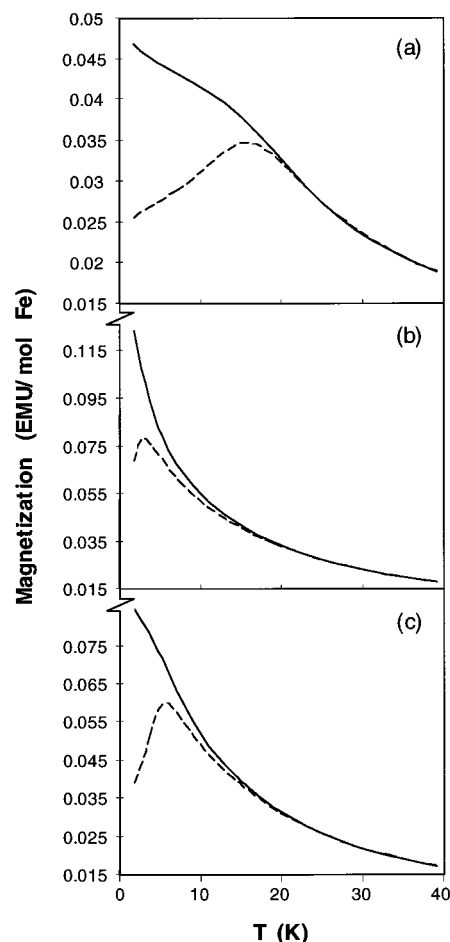
(31) Mohie-Eldin, M.-E. Y.; Frankel, R. B.; Gunther L. *J. Magn. Magn. Mater.* **1994**, *135*, 65.
(32) Bean, C. P; Livingston, J. D. *J. Appl. Phys.* **1959**, *30*, 120S.
(33) Mahmood, S. H.; Abu-Aljaraesh, I. *J. Magn. Magn. Mater.* **1993**, *118*, 193.

Figure 5. Zero-field-cooled (- - -) and field-cooled (—) magnetization as a function of temperature for three group III complexes at low applied field (250 G). (a) Fe(III)$_{6\pm\delta}$O$_x$(OH)$_y$(C$_{12}$H$_{25}$OSO$_3$)$_2 \cdot z$H$_2$O shows a blocking temperature, $T_{B(av)}$ near 16 K. (b) Fe(III)$_{3\pm\delta}$O$_x$(OH)$_y$(C$_{16}$H$_{33}$OSO$_3$)$_2 \cdot z$H$_2$O shows a much lower blocking temperature, $T_{B(av)}$ of only 3 K, indicating thinner layers in these complexes. (c) Thermal treatment of Fe(III)$_{3\pm\delta}$O$_x$(OH)$_y$(C$_{16}$H$_{33}$OSO$_3$)$_2 \cdot z$H$_2$O with H$_2$ results in an increase in blocking temperature ($T_{B(av)} = 6$ K), showing that this treatment can increase the domain size in these materials.

field, increasing the net magnetization. Higher values of T_B are associated with larger domains since the pinning of the domains to the lattice is a function of the domain volume.[31]

ZFC and FC magnetization curves for group III compounds are presented in Figure 5. Part a shows data obtained on a sample with six layers of iron oxide (thick layers). A peak in the ZFC curve is observed at 16 K, and the ZFC and FC curves are observed to converge at 21 K. These peak and convergence points can be assigned to the blocking temperatures of the average and largest domains in the samples, respectively.[31] In contrast, the data obtained on group III samples with only three layers of iron oxide (thin layers) show an appreciable reduction in the peak and convergence temperature. In this case, the peak and convergence temperatures are only 3 and 18 K, respectively. These data thus demonstrate the existence of smaller magnetic (and thus smaller structural) domains in the thin-layer iron oxide/surfactant composite compared to the thick-layer samples.

Similar phenomena can be observed in field-dependent magnetization hysteresis curves. Figure 6 shows hysteresis curves for samples with thin and thick iron oxide layers at 5 K. This temperature is above the average T_B for the thin-layer samples but below $T_{B(av)}$ for the thick layer samples. The thick-layer sample is thus observed to show hysteresis: that is, net remnant magnetization at zero applied field. Little hysteresis
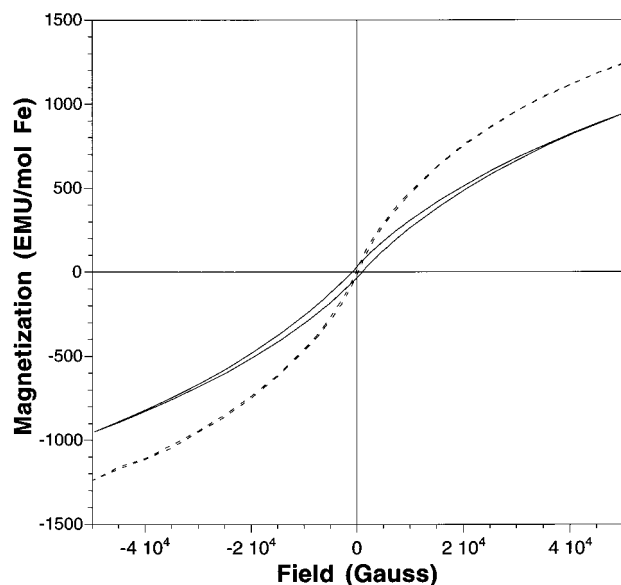
Figure 6. Hysteresis in a plot of magnetization versus applied magnetic field for two group III complexes at 5 K. This temperature is below the blocking temperature for Fe(III)$_{6\pm\delta}$O$_x$(OH)$_y$(C$_{12}$H$_{25}$OSO$_3$)$_2$·zH$_2$O (—), so hysteresis is observed. Little hysteresis is observed for Fe-(III)$_{3\pm\delta}$O$_x$(OH)$_y$(C$_{18}$H$_{37}$OSO$_3$)$_2$·zH$_2$O (- - -), however, as this compound is above its average blocking temperature of ca. 3 K.

is observed in the thin-layer sample which is above its average blocking temperature. Unblocked samples are expected to show magnetization which tracks the applied field.[32,34]

Mössbauer spectroscopy presents a final confirmation of the domain structure that has been suggested by magnetic susceptibility measurements. Variable-temperature ^{57}Fe Mössbauer spectra are presented in Figure 4 for a six (thick)-layer compound. At 38.4 K, a temperature above $T_{B(max)}$, a doublet is seen that is characteristic of a high-spin Fe^{3+} complex with an isomer shift (δ) of 0.37 mm/s (vs iron foil) and a quadrupole splitting (ΔE_Q) of 0.74 mm/s. No signal is observed from Fe^{2+} ions. As the temperature is decreased below $T_{B(max)}$, a sextet grows in the spectrum at the expense of the doublet. The sextet is first seen at 30 K, and at 9.1 K (below $T_{B(av)}$), only the sextet, with a magnetic hyperfine field of 435 kG, is seen. The presence of a sextet below 30 K is indicative of slow electronic relaxation of the Fe^{3+} ions in the sample relative to the Larmor frequency of the ^{57}Fe nucleus (ca. 10^7 s^{-1}). This slow flipping rate of unpaired spins results from magnetic exchange interactions between Fe^{3+} ions. Normally, multiple Fe^{3+} ions involved in exchange interactions (i.e., a magnetic domain structure) are needed to see sextet signals of this sort at temperatures as high as 30 K.[35,36] These results thus corroborate the conclusion drawn from magnetic susceptibility: group III compounds show cross-linked iron oxide (or oxy-hydroxide) layers with a magnetic domain structure.

A final experiment can be used to clarify the nature of the bonding in group III compounds. Because of the synthesis conditions used, the mostly likely structure for the iron species is an iron(III) oxy-hydroxide phase,[14] perhaps in combination with smaller, more highly hydroxylated iron clusters.[36] Thermal hydrogen treatment of the inorganic layers in these composites can be used to anneal this iron oxy-hydroxide phase, with two

possible outcomes: reduction of the FeO(OH) can result in the production of a mixed valent Fe(II)/Fe(III) oxide phase (Fe$_3$O$_4$) which is ferrimagnetic and thus should display improved magnetic properties. Alternatively, thermal hydrogen treatment can simply result in improved cross-linking of the iron oxide layers. Both of these results are desirable as both change the magnetic coupling within iron oxide layers and demonstrate that magnetic structure can be altered by chemical treatment after formation of the layered material. ZFC and FC magnetization curves for a three-layer (thin), group III sample that was treated with H$_2$/Ar (5/95) are shown in Figure 5 (bottom). In comparison to the untreated sample (Figure 5, middle), a clear shift in both the average and largest blocking temperature to higher temperature is observed [$T_{B(av)} = 6$ K, $T_{B(max)} = 19$ K]. The absolute magnitude of the molar susceptibility, however, does not appear to be significantly altered, indicating that the layers retain their FeO(OH) structure and have not been reduced to a mixed-valent Fe$_3$O$_4$ structure. As described above, this shift in T_B can be understood in terms of the development of larger magnetic domains in the H$_2$-treated material. The increase in the size of the magnetic domains can either be assigned to the development of larger iron oxide (or oxyhydroxide) domains or a reduction in defect density within the iron oxide domains. Further treatment of the inorganic layers or treatment under altered conditions could eventually convert the dominantly FeO(OH) layers into the ferrimagnetic structure, Fe$_3$O$_4$. Treatment with BH$_4^-$ salts is also a possibility for reduction of the Fe(III) ions and is being explored.

Thus a general structure for these group III materials can be written as Fe(III)$_{3\pm\delta}$O$_x$(OH)$_y$(C$_n$H$_{2n+1}$OSO$_3$)$_2$·zH$_2$O ($n = 16, 18$) and Fe(III)$_{6\pm\delta}$O$_x$(OH)$_y$(C$_n$H$_{2n+1}$OSO$_3$)$_2$·zH$_2$O ($n = 10, 12, 14$). The x, y, and z variables emphasize the fact that the exact nature of the iron−iron bridging is unknown and can be altered by chemical treatment.

IV. Discussion

Redox Chemistry and Layer Growth. A key feature of the synthesis of the materials described above is the use of redox chemistry to control the solubility of solution phase iron species. The general scheme employed is to create a salt-like nucleation site using simple ion exchange chemistry. By altering oxidation state, and thus solution phase solubility, iron oxide species become metastable in solution. Fe^{2+} ions do not readily form hydroxide complexes in solution and are thus significantly more stable than Fe^{3+} ions which readily hydrolyze to form solution phase hydroxide complexes followed by bulk precipitation of oxy-hydroxide materials. Precipitation into the already formed Fe/surfactant salt phase, however, is apparently kinetically favorable, compared to bulk FeO(OH) formation. The formation of nucleation sites prior to layer growth is thus key to this nonequilibrium approach to composite synthesis. Use of H$_2$O$_2$ as an oxidizing agent is also important in that it increases the pH slightly, a fact which further favors the aggregation of Fe-(III) into organized layered arrays. The hydrolysis of Fe(III) is known to be highly pH dependent, particularly at neutral or slightly acid pH.[37]

It should be emphasized that in all of these experiments Fe-(II) ions, which are quite stable in solution, are in large excess. In the syntheses of group III compounds, enough H$_2$O$_2$ is added to oxidize only about one-third to two-thirds of the Fe(II). Despite this fact, no Fe(II) is included in the surfactant composite materials, even when syntheses are carried out under inert atmosphere. This fact emphasizes the notion that it is the

(34) Ziolo, R. F.; Giannelis, E. P.; Weinstein, B. A.; O'Horo, M. P.; Gang uly, B. N.; Mehrotra, V.; Russel, M. W.; Huffman, D. R. *Science* **1992**, *257*, 219.

(35) *Applications of Mössbauer Spectroscopy*; Cohen, R. L., Morup, S., Eds.; Academic Press: New York, 1980; Vol. II.

(36) Mitov, I.; Tabakova, T.; Andreeva, D.; Tomov, T. *Z. Phys. D* **1991**, *19*, 275.

(37) *The Hydrolysis of Cations*; Baes, C. F., Mesmer R. E., Eds.; John Wiley & Sons: New York, 1976; pp 226−237.

oligomerization and related reduced solubility of Fe(III) species which drives the formation of the group III composites described above.

A unique feature of these materials is the ability to make iron oxide surfactant composites with different, but homogeneous layer thicknesses. In the case of group I and II compounds, control over layer thickness is achieved by controlling the starting material [either Fe(II) or Fe(III)]. In the case of group III compounds, layer thickness is controlled by diffusion and strain. When surfactants with shorter chain lengths (10, 12, or 14 carbons) are employed, the structures are apparently more open and Fe(III) species can more readily diffuse into the layers. After formation of approximately six iron oxide (or oxy-hydroxide) layers, however, the inorganic layer growth stops. This abrupt termination of growth could be due to strain in the composite caused by a mismatch between the ideal surfactant chain packing and the ideal iron spacing. This strain could result either in termination of layer growth or in phase separation (i.e., bulk FeO(OH) precipitation) when a critical layer thickness is exceeded. Alternatively, the thickness could be controlled purely by diffusion: as the iron oxide layer grows, the composite is pulled more tightly together and diffusion of Fe(III) species is stopped. Both of these alternatives are consistent with the observation that for 16- and 18-carbon surfactants, which should have stronger van der Waals interactions between tails, only about three layers of iron oxide or oxy-hydroxide are formed. Both the strain caused by trying to distort ideal chain packing and the overall chain packing density should be higher in these materials compared to those made with shorter chain surfactants.

The fact that only two different layer thicknesses are formed (ca. three or ca. six Fe oxy-hydroxide layers), as opposed to a continuum of increasing layer thickness with decreasing surfactant chain length, suggests that the formation of group III compounds is also a cooperative process. This phenomenon is not well understood, and in particular, the special stabilization of the two layer thicknesses that are observed here is not obvious. The idea of cooperative layer growth, however, is supported by the fact that as H_2O_2 is added to the Fe(II)/surfactant salts, gradual layer growth is also not observed. Instead, addition of insufficient H_2O_2 results in a mixed population of group I and group III compounds. Additional H_2O_2 converts further group I material to group III, suggesting that individual domains undergo structural change together. This is reasonable, since once an iron oxide layer is "opened-up" by the precipitation of Fe(III), further Fe(III) precipitation is facilitated. This type of cooperative layer growth is surely another key feature for the production of well-defined layer thicknesses by kinetically controlled hydrolysis and precipitation.

Superparamagnetism and Superantiferromagnetism. Up to this point, we have used the term "superparamagnetism" to describe the unblocking of the magnetic domains in these materials above T_B. The term superparamagnetism, however, is meant to describe very small domains of ferromagnetic material that act like single, large paramagnets.[32] As we have concluded on multiple occasions, however, the magnetic coupling in these surfactant/inorganic composites is dominantly antiferromagnetic. The proper term to describe these materials is thus "superantiferromagnetism."[31,38] Superantiferromagnetism, like superparamagnetism, refers to small, coupled domains that are not pinned to the lattice at temperatures above T_B. The dominant coupling in superantiferromagnetic domains

is antiferromagnetic. Because of the finite size and large surface area of the domains, however, many spins cannot be paired. The net magnetization in superantiferromagnetic materials thus arises mainly from these unpaired interfacial spins; as a result, the overall magnetization of superantiferromagnetic domains is much lower than superparamagnetic domains.

The unpaired spins in superantiferromagnetic domains are locked (orientationally) to the whole antiferromagnetic domain. That is to say, regardless of whether the spins are locked to the atomic lattice (i.e., $T > T_B$ or $T < T_B$), the spins in the entire domain retain a fixed orientation with respect to each other.[38] Thus, despite the fact that the magnetization observed in Figure 5 arises from only a small fraction of the Fe(III) ions of the composite, the blocking temperatures at low applied fields are a measure of the overall domain size.

One of the initial goals of this work was to use simple chemical processes such as self-assembly and redox chemistry to produce large amounts of potentially useful nanoscale magnetic (i.e., superparamagnetic or ferromagnetic) materials. Possible uses include magnetic storage, giant magnetoresistance (GMR), or any application that utilizes coupling between nanoscale magnetic domains. Because both the interlayer spacing and the iron oxide layer spacing can be easily varied, this type of coupling could be tuned for specific applications. While the work presented here is an important first step toward this goal, these materials are significantly limited with respect to achieving this goal by the predominance of antiferromagnetic coupling within the iron oxy-hydroxide layers. To remedy this problem, two methods are immediately obvious: posttreatment of samples at moderate temperatures have been shown to increase the domain size in the iron oxide layer. Treatment of bulk FeO(OH) samples with pure H_2 at high temperatures has been shown to convert FeO(OH) to Fe_3O_4, which is ferrimagnetic. While these composites are not stable under those bulk reducing conditions, it is possible that alternate reducing agents or electrochemistry can be used to accomplish the same transformation. Alternatively, solution phase conditions which favor the formation of Fe_3O_4 (mixed Fe(II) and Fe(III)), γ-Fe_2O_3 (pure Fe(III)), or other ferrimagnetic mixed-metal spinels directly could be found. One example of this which is currently being investigated in our laboratories is the synthesis of $MnFe_2O_4$ composites starting with a Mn^{2+} group I material and treating this with H_2O_2 in the presence of excess Fe^{2+}. The general method of coupling surfactant self-assembly with inorganic iron oxide precipitation remains an attractive route for the simple production of ordered nanoscale magnetic materials.

Overview of Composite Structure. An overview of the synthetic scheme described in this manuscript is presented in Figure 7 for group I and group III compounds. This diagram is constructed to best include information obtained from both structural and magnetic structure measurements. The initial Fe-(II) salt phase is shown in the middle left. This material is depicted as a hydrated layered (lamellar) salt with only electrostatic interactions between the inorganic and organic species. The chains are packed with interdigitated surfactant carbon atom chains in a paraffin-like monolayer structure. Upon dehydration (moving to the left), two main changes are observed. The loss of water molecules cause the headgroups to pack much more closely together, possibly allowing for better chelation of the iron ions by the sulfate headgroups. This close packing of the headgroups is not compatible with the paraffin-like monolayer observed in the hydrated samples, so the tails rearrange to form a paraffin bilayer. A similar sequence of events is expected for dehydration of group II compounds, although in

(38) Néel, L. In *Low-Temperature Physics, Summer School of Theoretical Physics, Les Hauches 1961*; Dewitt, C., Dryfus, B., Eds.; Gordon and Breach: New York, 1962.
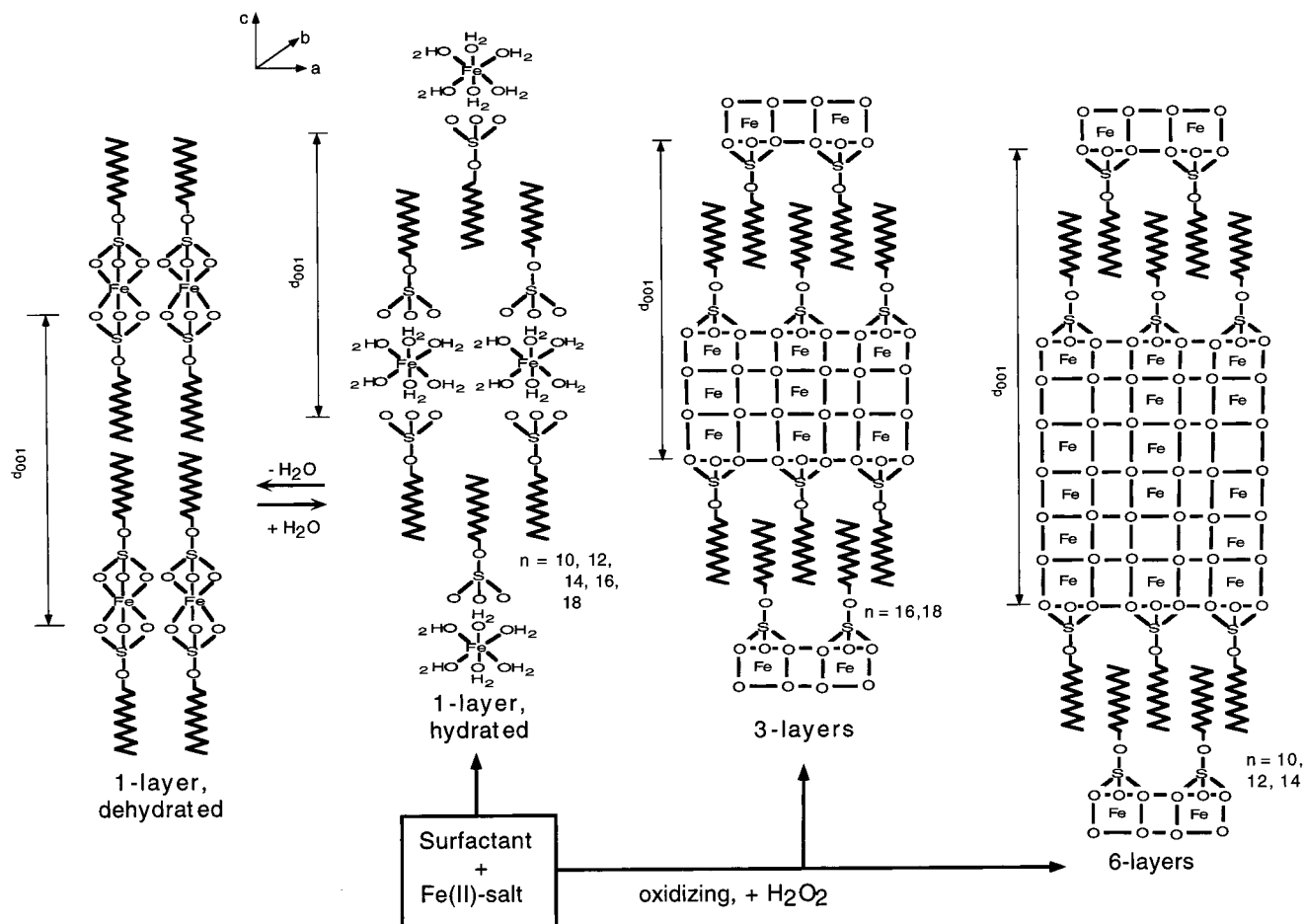
Figure 7. Schematic representation of the formation of group I and group III compounds. Group I compounds are salt-like and thus show a change in surfactant structure upon dehydration (moving to the left). Addition of H_2O_2 to group I salts (moving to the right) produces group III compounds which appear to consist of cross-linked, dominantly FeO(OH) types layers in alternation with surfactant bilayers. The iron oxide layer thickness depends on the surfactant chain length with shorter surfactant chains producing thicker iron oxide layers.

this case, the inorganic species is expected to be a μ-oxo-bridged Fe_2O^{4+} species. Atomic scale ordering is observed in hydrated group I compounds, but in dehydrated group I and all group II compounds, only poorly defined diffraction peaks are observed at high angles in XRD, despite well-defined lamellar order with superatomic periodicity.

Upon oxidation (moving to the right in Figure 7), Fe(III) is precipitated into layered arrays, thus forming the inorganic region of the composites. This produces a cross-linked iron oxy-hydroxide layer which no longer shows structural change upon dehydration. Starting with surfactants containing 16- or 18-carbon chains, a composite with approximately three iron oxide layers is formed (Figure 7, middle right). When shorter surfactant molecules are used (with 10, 12, or 14 carbon atoms), composites containing close to six layers of iron are observed (Figure 7, far right). The structure of the iron oxide material is depicted as FeO(OH). Defects and vacancies have been included, however, to indicate that the inorganic layers are not in the form of perfect FeO(OH) sheets of exact thickness. The data suggest that finite domains are formed containing a number of unpaired Fe(III) ions, and thus, polycrystalline sheets or agglomerated nanoclusters are the most likely form for the layers. The domain size is strongly correlated to the overall layer thickness, however, with larger domains observed in the thicker samples.

V. Conclusions

In this paper, we have presented a procedure to use redox chemistry and the variable solubility of iron ions in solution to form lamellar iron oxide/surfactant composites with a controllable inorganic layer thickness. These materials display super-antiferromagnetism and mark an important first step toward the simple design of hierarchically ordered nanoscale magnetic materials by a combination of organic self-assembly with inorganic precipitation. Further work in this area will focus on improved control of the inorganic oxidation states and thus improvement of the magnetic properties of the materials.

This general synthesis method, however, is potentially applicable to a variety of other systems. Any system which contains an accessible oxidation or reduction transition which is accompanied by a dramatic change in solubility can potentially be used. Chemical changes are also not limited to oxidation or reduction. For instance, the slow release of base to change the solubility of aluminum cations in the synthesis of hexagonal alumina/surfactant composites[39] and the addition of phosphate to Ca/surfactant liquid crystals recently employed in the synthesis of layered calcium−phosphate/surfactant composites[40] can be considered other examples of the same phenomena. Changes in chelation, charge density, or clustering with appropriate kinetic control can all potentially be used to precipitate inorganic materials into organic/inorganic composites. As long as inorganic precipitation is dominated by the presence of nucleation sites (which is required to avoid bulk precipitation), this synthetic method should be generally applicable.

(39) Yada, M.; Machida, M.; Kijima, T. *Chem. Commun.* **1996**, 769.
(40) Varaksa, N.; Kuperman, A.; Ozin, G. A. *Chem. Mater.* **1996**, *8*, 1084.

Table 3. Synthesis Conditions for Group I, II, and III Compounds

compd	mmol of surf[a]	vol of surf soln (mL)	mmol of Fe(II or III)	vol of Fe soln (mL)	mixing temp	mL 0.88 mol·L^{-1} H$_2$O$_2$
I & III, C-10	1.0	20	10	40	rt	4
I & III, C-12	1.0	20	10	40	rt	4
I & III, C-14	1.0	40	10	40	≈40 °C	4
I & III, C-16	0.5	40	10	40	≈50 °C	2
I & III, C-18	0.5	40	10	40	≈60 °C	2
II, C-12	1.0	40	10	40	rt	
II, C-14	1.0	40	10	40	≈40 °C	
II, C-16	0.4	40	10	40	≈50 °C	
II, C-18	0.4	40	10	40	≈60 °C	

[a] surf = surfactant.

Appendix: Detailed Synthesis

In the most straightforward syntheses, group I and II compounds were formed by mixing a homogeneous FeCl$_2$ or FeCl$_3$ solution with a well-dissolved sodium sulfate surfactant solution. Exact molar quantities and volumes are listed in Table 3. In most cases, the surfactant solutions were heated to increase the dissolution rate. For 14-, 16-, and 18-carbon chain surfactants, the Fe solutions and the surfactant solutions were mixed while the surfactant solutions were still warm as precipitation of the pure surfactant occurred at room temperature and the concentrations used in the experiments. Mixing temperatures are given in Table 3. Group I and II compounds were allowed to stir for approximately 1 h before being filtered and washed with water. Group I compound were synthesized entirely under Ar atmosphere and were not exposed to air until the compound was filtered and completely dried. Group II compounds were synthesized in air. Group III compounds were synthesized from group I compounds by the addition of 0.88 mol·L^{-1} fresh H$_2$O$_2$. Volumes required for complete conversion of group I to group III are given in Table 3. Group III compounds were allowed to sit at room temperature under inert atmosphere overnight before being filtered in air, washed with water, and dried under reduced pressure.

It should be noted that, while exact concentrations are presented in Table 3, the syntheses were not particularly sensitive to any values other than the ratio of H$_2$O$_2$ to surfactant, and even this ratio could be varied. Too little H$_2$O$_2$ always resulted in a mixed group I/group III population. Some excess H$_2$O$_2$, however, merely produced solution phase Fe(III), while bulk FeO(OH) was only generated when a large excess of H$_2$O$_2$ was utilized. Significant dilution of the reaction mixtures compared to that presented in Table 3 could also prevent precipitation of the group I and II salts. Concentrations up to 10-fold, however, appeared to have little effect on the reaction. Additionally, as long as Fe cations were present in sufficient excess, the exact Fe:surfactant molar ratio was not critical.